Chemical Physics 365 (2009) 69–79

Contents lists available at ScienceDirect

Chemical Physics

journal homepage: www.elsevier.com/locate/chemphys

# Is the C=O frequency shift a reliable indicator of coumarin binding to metal ions through the carbonyl oxygen?

Ivelina Georgieva [a,*], Natasha Trendafilova [a], Bernadette S. Creaven [b], Maureen Walsh [b], Andy Noble [b], Malachy McCann [c]

[a] Institute of General and Inorganic Chemistry, Bulgarian Academy of Sciences, 11 Acad. G. Bonchev Str., Sofia, Bulgaria
[b] Department of Applied Science, Institute of Technology, Tallaght, Dublin 24, Ireland
[c] Department of Chemistry, National University of Ireland, Maynooth, Co. Kildare, Ireland

ARTICLE INFO

*Article history:*
Received 1 July 2009
Accepted 7 October 2009
Available online 13 October 2009

*Keywords:*
Ag(I)
Cu(II) complexes
Coumarin
DFT modeling
Electronic structure
IR spectra

ABSTRACT

The coumarin ligand, 4-hydroxy-3-nitro-*2H*-chromen-2-one (*Hhnc*) and its Cu(II) and Ag(I) complexes were studied by DFT calculations at B3LYP/B1 and PW91/B1 levels. MEP of the deprotonated ligand, $hnc^-$, and energy calculations of model metal complexes predicted the ligand binding to the metal ion through the hydroxyl and the nitro oxygens in agreement with experiment. Based on precisely selected Cu/Ag model complexes with $hnc^-$, a relation between the vibrational behaviour of the ligand donor groups and the ligand binding modes in the complexes was deduced. The observed carbonyl $\nu$(C=O) downshift (50–90 $cm^{-1}$) is attributed to intermolecular H-bonding formed between the C=O group and lattice water molecules or due to the C=O binding to the metal ion in case of bridging coumarin ligand (in Aghnc). Much larger $\nu$(C=O) downshift (~220–240 $cm^{-1}$) is predicted in case of monodentate or bidentate (with the nitro group) bonding of the carbonyl C=O group to the metal ion.



## 1. Introduction

Coumarin is a benzopyrone that occurs naturally in many plants and essential oils. For many years coumarin derivatives have attracted much attention because of their applications in new technologies due to their photochemical and photobiological properties [1–3] and in pharmacology and medicine due to their anticoagulant [4], anti-bacterial [5,6], cytotoxic [7–10], antifungal [11,12], anti-inflammatory [13], anti-thrombotic and vasodilatory [14], and anti-mutagenic [15] activities. With the aim of discovering more potent and selective bioactive coumarin agents the researchers have carried out investigations in two fields: synthesis of new coumarin derivatives and synthesis of metal complexes of coumarins. Many studies have already proven that the coordination of metal ions to therapeutic coumarin agents improve their efficacy and accelerates the bioactivity [16–21]. Due to the importance of coumarins and their metal complexes for medicine and photobiology they have been widely investigated both from experimental [22] and theoretical [23–25] viewpoints. Transition metals (Cu(II), Ag(I), Pt(II), Sn(IV)) and lanthanides (Ln(III) and Zr(IV)) are of special interest because their salts possess therapeutic potential. It is thought that the therapeutic potential of coumarin ligands is enhanced when they are bonded to such metals. It is interesting to clarify the effect of the metal type, oxidation state and binding mode on the therapeutic or thermodynamic properties of coumarins. At the same time, the successful development of biologically active metal–coumarin complexes requires well known correlation between the geometrical and electronic structures of the complexes from one side and their bioactivities from the other. When X-ray data are not available, the vibrational (IR and Raman) spectroscopy could help the structure recognition. The interpretation of the observed coumarin IR spectra is however a challenge because of (1) abundance of IR bands in the spectra, (2) presence of more than one donor atoms and possibility of various binding modes, and (3) coumarin donor groups are involved in a conjugated system and H-bondings. The modeling of coumarins and their metal complexes, including calculations of their vibrational spectra and comparison with the experimental ones, is a powerful approach for reliable interpretation of the available IR data and for prediction of the coumarin binding mode to metals [24,26,27]. With the help of geometry and frequency calculations of coumarin derivatives it has been shown that the downshifts of the carbonyl and carboxylic C=O stretching frequencies observed on going from the ligand IR spectrum to the metal complex spectrum is not a direct indication of a metal coordination to the corresponding groups [26,27]. The active ligand form in the complexation reaction is the deprotonated one, which is experimentally inaccessible. The calculations predict quite different IR spectra of the neutral and deprotonated ligand forms. The IR spectrum of the deprotonated form

* Corresponding author.
*E-mail address:* ivelina@svr.igic.bas.bg (I. Georgieva).

0301-0104/$ - see front matter © 2009 Elsevier B.V. All rights reserved.
doi:10.1016/j.chemphys.2009.10.004

functions as the real reference for comparison and interpretation of the IR spectra of its metal complexes. Our previous calculations revealed an interesting vibrational behaviour of some coumarin vibrational modes in the metal complex spectra. Due to the conjugated coumarin system, the coordination of the metal to one donor group (for example hydroxyl C–O) induces polarization in the lactone ring and hence a significant shift in the free carbonyl stretching frequency [23,24,26,27]. The aim of the present study is to elucidate the vibrational behaviour of the coumarin ligand, 4-hydroxy-3-nitro-*2H*-chromen-2-one in metal complexes and to derive a vibrational criteria capable to distinguish (1) the coumarin (*hnc*$^-$) binding modes in Cu(II) and Ag(I) complexes and (2) the H-bonded from metal-bonded carbonyl group. For that purpose we performed DFT modeling of the geometrical and electronic structure and vibrational properties of the neutral (*Hhnc*) and deprotonated (*hnc*$^-$) ligand, as well as of the model and real (according to the X-ray data) Ag(I) and Cu(II) complexes of *hnc*$^-$.

## 2. Computational details

The geometry and frequency calculations of *Hhnc*, *hnc*$^-$, Ag(*hnc*), [Cu(II)(*hnc*)]$^+$/Cu(I)(*hnc*), Cu(*hnc*)$_2$($H_2O$)$_2$ and Cu(*hnc*)$_2$($H_2O$)$_2$·2$H_2O$ were carried out with DFT method using Gaussian03 program [28]. All calculations were done using a tight geometry criterion (the convergence criterion for rms deviations in electron density matrix elements of the SCF algorithm is of $10^{-8}$ a.u.). Basis set 6-31G(d) (split valence plus polarization basis set) was applied for main group elements: for hydrogen atoms (4s)/[2s]), for carbon, oxygen and nitrogen atoms (10s4p1d)/[3s2p1d]. Furthermore, to give a better description of the wave functions in the intermolecular region and hence, to satisfy estimation of the M-hnc interactions, diffuse functions were added to the standard basis set (one s and one p set) for the O atoms and the final basis set was (11s5p1d)/[4s3p1d]. The combined basis set is denoted as B1. The computations using B1 basis set were carried out with the Lee, Yang, and Parr correlation functional (LYP) [29] combined with Becke's three parameters exchange functional (B3) [30]. The adequacy of B3LYP method for prediction of conformational behaviour, geometry parameters and vibrational spectra of coumarin derivatives was proven in our recent investigation [24]. The metal ions were calculated with the relativistic effective core potential (RECP) optimized by the Stuttgart–Dresden group [31]. The small core RECPs (SDD) were used for Cu(II) (MDF10) [32] and Ag(I) (MWB28) in combination with their optimized valence basis sets (8s7p6d)/[6s5p3d] throughout this paper. The small core (RECPs) for the Cu(II) and Ag(I) centers considers explicitly 19 valence electrons ($3s^23p^63d^{10}4s^1$ (Cu) and $4s^24p^64d^{10}5s^1$ (Ag)), whereas 10 core electrons ($1s^22s^22p^6$ shells) for Cu(II) and 28 core electrons ([Ar]$3d^{10}$ shells) for Ag(I) are replaced by the pseudopotential. The reliability of ECP to describe Cu was tested versus B3LYP/6-311+G(d) calculations (all electrons are treated). A comparison of the calculated geometry parameters of [Cu(hnc)]$^+$ with small ECP and B3LYP/6-311+G(d) basis set for Cu(II) showed close results and the differences vary from 0.001 to 0.006 Å.

Full geometry optimizations of all the molecular systems were carried out without symmetry constraint. The minima on the potential energy surfaces were qualified by the absence of negative eigenvalues in the diagonalized Hessian matrix, giving imaginary normal vibrational mode. The projection of internal coordinates onto each normal mode in terms of percentage relative weights was computed as implemented in Gaussian03. Each normal mode is described on the basis of the largest percentage value of the total displacement vector magnitude. In addition, the vibrational modes have been analyzed by visual inspection of modes animated using the ChemCraft program [33]. The calculated IR spectra were visualized using Doppler broadening and band width on half height of 80. To distinguish the deprotonated O1, coumarin carbonyl O4 and coumarin cyclic O5 atoms, forming CO bonds in *hnc*$^-$ (Fig. 1b) we designated them as hydroxyl O1, carbonyl O4 and cyclic O5 atoms and groups, respectively.

The periodic density functional theory (DFT) calculation of polymeric Aghnc is performed using the Vienna Ab initio Simulation Package (VASP) [34]. The DFT is parameterized in the local-density approximation (LDA), with the exchange–correlation functional proposed by Perdew and Zunger and corrected for non-locality in the generalized gradient approximations (GGA) using Perdew–Wang91 (PW91) functional. The interaction between the core and the electrons is described using the PAW (projector augmented wave) potentials for all atoms.

## 3. Results and discussion

### 3.1. Donor ability and binding properties of the *hnc*$^-$ ligand in model metal complexes

According to the experiment [22], the active ligand form in complexation reaction with metal ions is the anionic *hnc*$^-$ form, which arises from deprotonation of the hydroxyl group, Fig. 1. The anionic ligand contains three donor groups: hydroxyl, carbonyl and nitro and five potential reactive centers for coordination to metal presupposing five binding modes in metal complexes. X-ray diffraction analyses of Cu(II) and Ag(I) complexes of *hnc*$^-$ revealed two different ligand binding modes: bidentate through the hydroxyl and nitro oxygens (in both complexes) and monodentate through the carbonyl O (in Ag(I) complex) [22]. To clarify the factors responsible for the coordination ability of *hnc*$^-$ we calculated molecular electrostatic potential (MEP) of the ligand and energies of various model complexes.

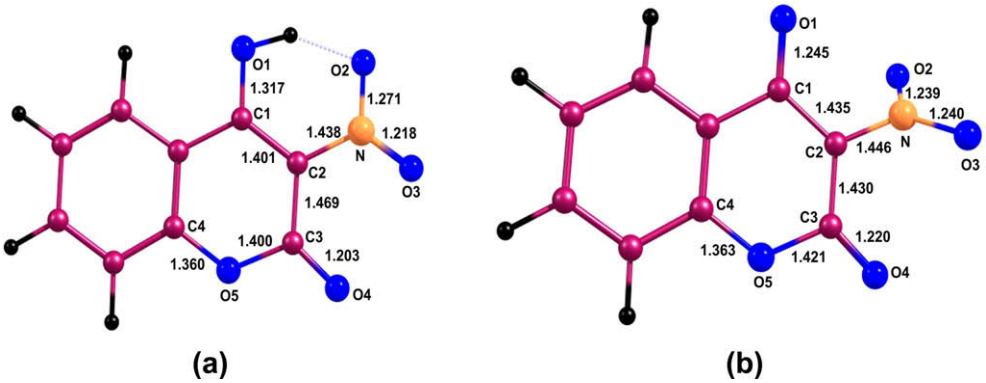


**Fig. 1.** Optimized geometries at B3LYP/B1 level of (a) neutral (*Hhnc*) and (b) deprotonated (*hnc*$^-$) ligand.

The optimized *Hhnc* structure at B3LYP/B1 level is a minimum in $C_s$ symmetry stabilized by one intramolecular H-bond, whereas the $hnc^-$ structure is a minimum in $C_1$ symmetry, Fig. 1. In $hnc^-$, the N–O2 and N–O3 bond lengths are very close and the nitro group is twisted with respect to the plane of the coumarin ring (the dihedral angle C1–C2–N–O2 is −49.29°).

The reactive sites in $hnc^-$ for electrophilic attack (metal ions) are estimated by means of molecular electrostatic potential calculations. MEP at a given point $r(x, y, z)$ in the vicinity of the molecule is defined in terms of interaction energy between the electrical charge generated from the molecule electrons and nuclei and the positive test charge (a proton) located at $r$. The MEP values are calculated on a molecular surface defined by electron density 0.001 e/bohr$^3$ [35,36]. 3D MEP contour map of $hnc^-$ is presented in Fig. 2 (the surface clipping plane coincides with the plane of the coumarin ring). The most favorable regions for electrophilic attack are those corresponding to the minima of the electrostatic potential values. As it is seen from Fig. 2, there are three regions with large negative values: between O1 and O2 atoms (denoted as $V_1$), between O4 and O3 (denoted as $V_2$) and between O2 and O3 (de-

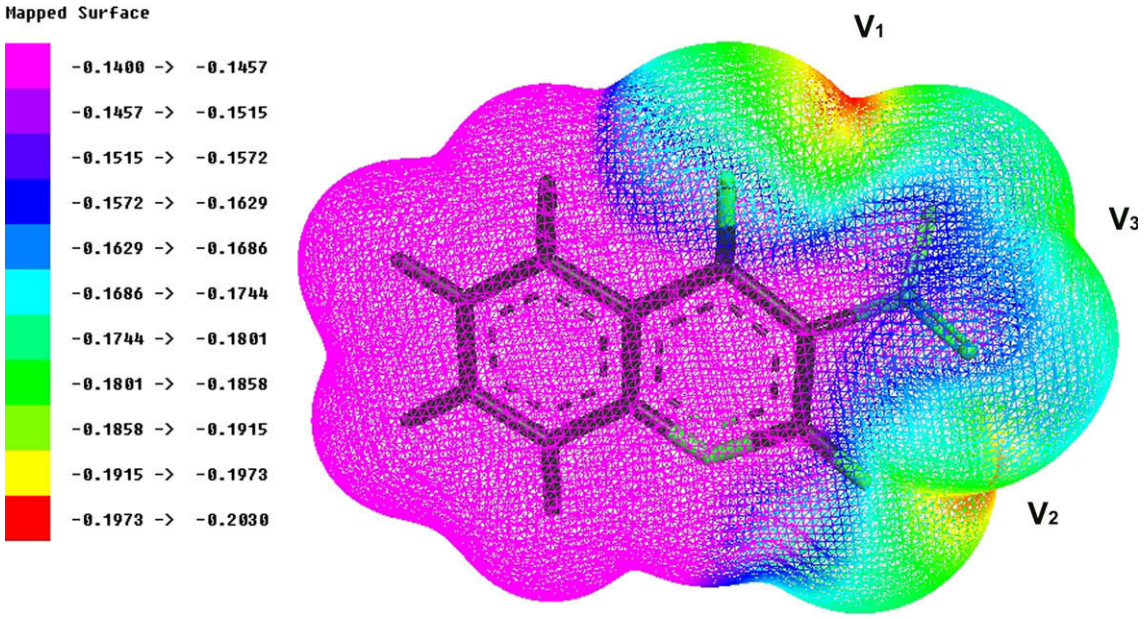


**Fig. 2.** Molecular electrostatic potential of $hnc^-$, mapped on molecular surface defined by electron density $\rho(r) = 0.001$ e/bohr$^3$.

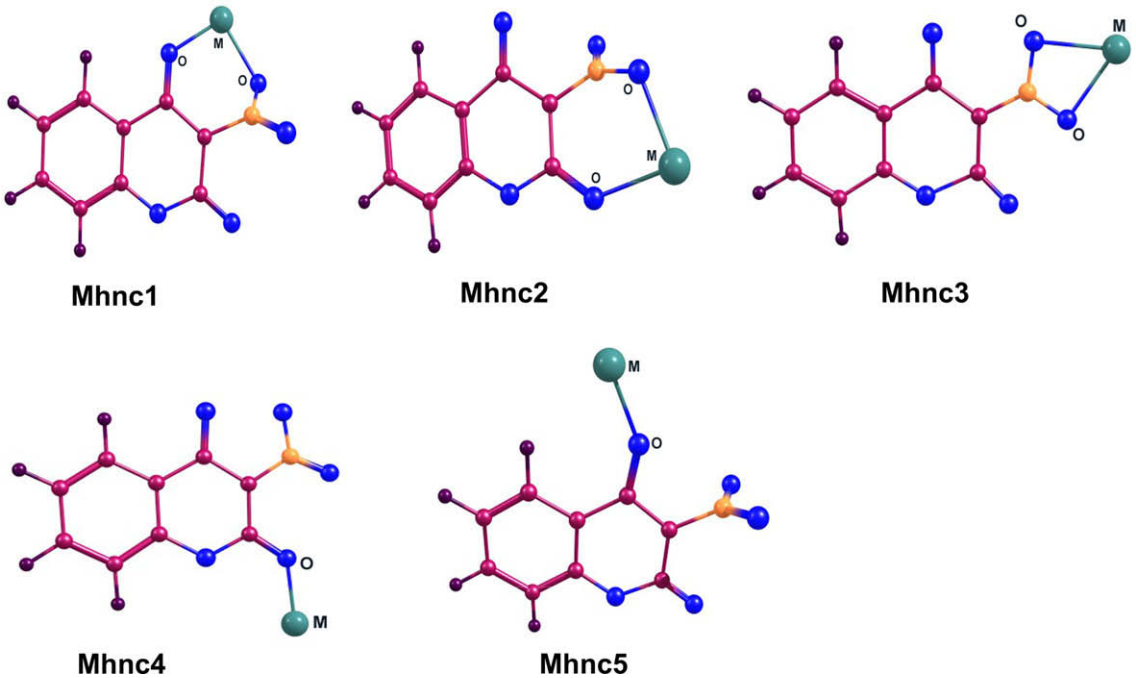


**Fig. 3.** Schematic presentation of the possible ligand binding modes to transition metals.

noted as $V_3$). The suggested regions could not be attributed to definite atoms of the molecule. According to the MEP values, the most reactive region in *hnc*$^-$ is $V_1$ (−0.2020 a.u.), followed by $V_2$ (−0.1965 a.u.) and $V_3$ (−0.1790 a.u.). Hence, the MEP results pre-

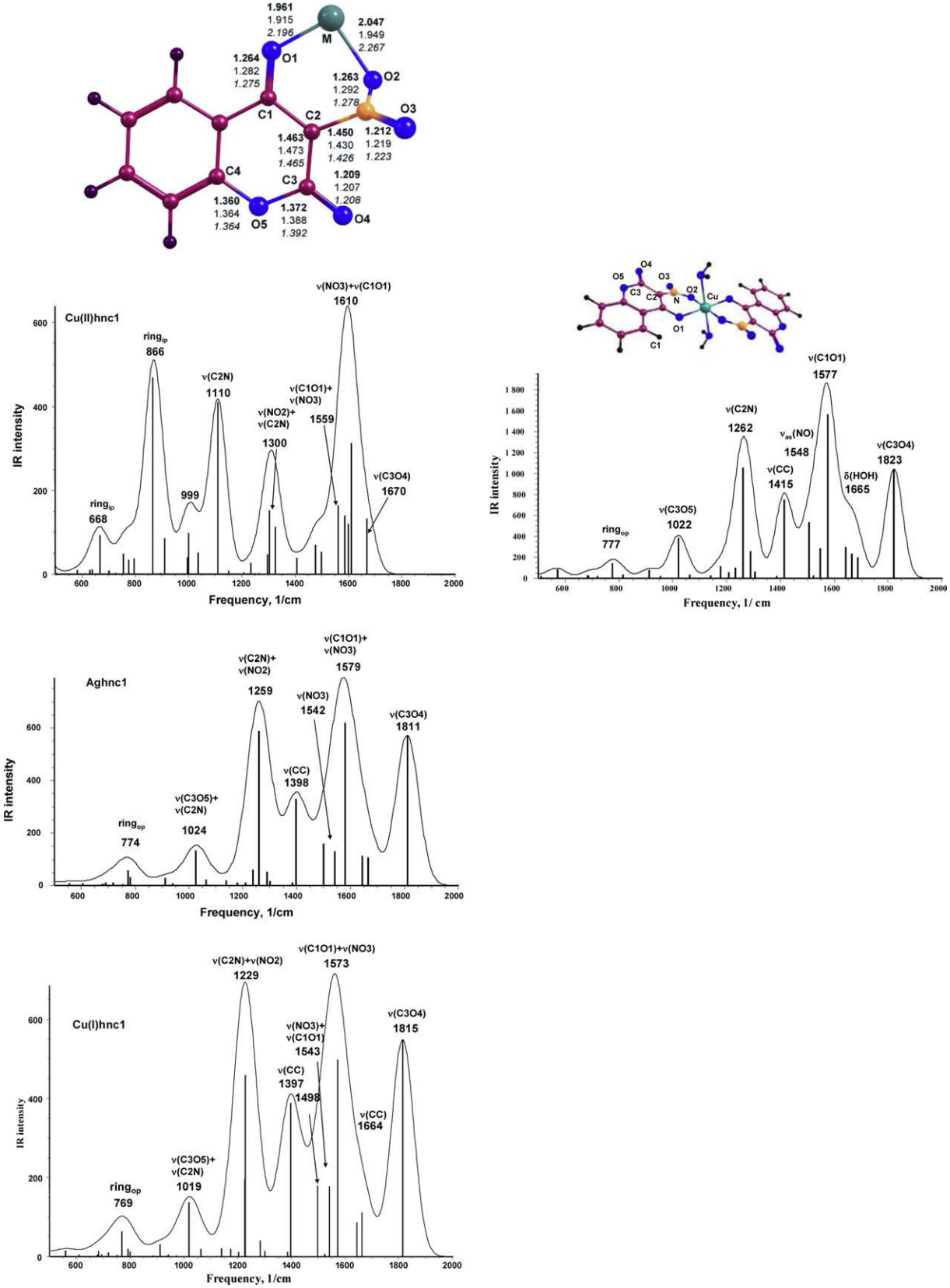


**Fig. 4.** Selected calculated bond lengths and IR wavenumbers (unscaled) of the optimized Mhnc1 model complexes (M = Cu(II) (**bold**), Cu(I) (regular), Ag(I) (*italic*)).

dict bidentate binding through the hydroxyl O1 and nitro O2 atoms. The MEP prediction is in line with X-ray diffraction analysis data for Cu(II) complex which have shown only this mode of binding [22]. For Ag(I) complex of *hnc*$^-$ the experiment has shown two binding modes of the ligand: bidentate binding through the hydroxyl O1 and nitro O2 atoms (as in the case of Cu(II)) and monodentate binding to Ag(I) through the carbonyl O4 [22]. To gain more insight into the coordination behaviour of *hnc*$^-$ to Ag and Cu ions, the possible bidentate and monodentate complexes (M:L = 1:1) are modeled as shown in Fig. 3. The bidentate ligand binding could be realized through the (1) hydroxyl O1 and nitro O2 (Mhnc1); (2) carbonyl O4 and nitro O3 (Mhnc2); (3) nitro O2 and nitro O3 (Mhnc3). The monodentate ligand binding could be through the (1) carbonyl O4 (Mhnc4) and (2) hydroxyl O1 atom (Mhnc5). The model complexes are used for qualitatively suggestions of the preferred binding ligand mode in Cu(II) and Ag(I) complexes. The relative stabilities of five [Cu(II)hnc]$^+$, four [Ag(I)hnc] and four [Cu(I)hnc] model complexes are evaluated on the basis of their electronic energies, Table S1 in Supplementary materials. For all systems studied, the most stable structure is Mhnc1, where the *hnc*$^-$ is bidentately bonded through the hydroxyl O1 and nitro O2 atoms. The same bidentate binding of *hnc*$^-$ was predicted from MEP calculations and confirmed from the experiment [22]. The agreement between the observed coordination of *hnc*$^-$ in the metal complexes and the predicted bidentate (O1, O2) ligand binding in model complexes support the reliability of the models applied. The bidentate binding through O4 and O3 atoms produces less stable structures (with 2–4 kcal/mol). As it is expected, the bidentate binding structures are more stable than the monodentate one. This result excludes the single monodentate *hnc*$^-$ coordination, however it could occur in combination with bidentate one, as it was observed in the Ag complex [22].

### 3.2. Vibrational properties of mono- and bidentate binding modes of model [Cu(II)hnc]$^+$, Cu(I)hnc and Ag(I)hnc complexes

The experimental structure of Aghnc shows that in addition to the most probable bidentate O1, O2-hnc binding, monodentate O4-hnc binding is also realized [22]. To derive the characteristic vibrational properties of the ligand, which are related to its coordination behaviour in the Cu and Ag complexes, we calculated the IR spectra of the model complexes shown in Fig. 3. The calculated bond lengths and the vibrational spectra of the optimized Mhnc1 complexes (M = (Cu(II), Ag(I), Cu(I)) are given in Fig. 4. Our discussion is mainly concentrated on the vibrational behaviour of the donor groups C1O1, $NO_2$, C3O4 and their neighbors C2N, C3O5. The stretching modes of the bonds above exhibit very intense IR bands and their positions could reveal the binding behaviour of the ligand.

To test the reliability of the selected model complexes ([Cuhnc1]$^+$ and Aghnc1), their calculated vibrational spectra are compared to those of real neutral complexes ($Cu(hnc)_2(H_2O)_2$ and Aghnc). The comparison shows that the IR spectra of the model [Cuhnc1]$^+$ and $Cu(hnc)_2(H_2O)_2$ complexes differ significantly, Fig. 4. At the same time, the calculated IR spectrum of Cu(I)hnc is very similar to the IR spectrum of $Cu(hnc)_2(H_2O)_2$. A detail electronic structure analysis of the Cu complexes suggested that the similarity of the IR spectra of $Cu(hnc)_2(H_2O)_2$ and Cu(I)hnc complexes is related to the similar character of the orbital interactions, Fig. 5a and c, the destabilized 3d copper orbital interacts with the hydroxyl and nitro oxygen orbitals. Differently, for [Cu(II)hnc]$^+$ the highest 3d$\sigma$ orbital is stabilized and the preferred situation corresponds to singly occupied orbital on *hnc*, Fig. 5b. Similar findings have been reported in previous studies on Cu(II) complexes [37,38]. In $Cu(hnc)_2(H_2O)_2$ and [Cu(I)hnc] the spin delocalization is between metal and ligand orbitals, whereas in [Cu(II)hnc]$^+$ the spin is localized on the ligand. Therefore, in Cu(II) complexes with coumarins, the change of the coordination environment produces different metal–ligand orbital interactions and therefore the Cu(II):hnc = 1:1 is unsuitable model for vibrational study.

Further, Aghnc and Cuhnc models are used to estimate the relation between the ligand binding mode and the vibrational spectral features of the metal complexes. The calculated geometries and vibrational spectra of Cuhnc binding models are presented in Fig. 6, whereas all Cu(II), Cu(I) and Ag(I) model complexes are compared in Fig. S1 in Supplementary materials. As it is seen in Fig. 6, the first two intense bands in the 2000–500 cm$^{-1}$ IR range of the complexes studied are assigned to carbonyl $\nu$(C3O4) and hydroxyl $\nu$(C1O1) modes. Their order varies: in the case of uncoordinated carbonyl C3O4 group in the Cuhnc1 and Cuhnc3, the $\nu$(C3O4) band appears as the first one and in the case of coordinated C3O4 group in Cuhnc2 and Cuhnc4, the $\nu$(C3O4) band is the second one. The $\nu$(C3O4) and $\nu$(C1O1) band intensities also vary in the complexes studied: more intense is the band of the coordinated CO group. The bidentate O3,O4-Cuhnc2 and monodentate O4-Cuhnc4 complexes show very similar $\nu$(C3O4) and $\nu$(C1O1) vibrational behaviour and therefore the vibrational spectra could not be used to distinguish the complexes. In such a case, thermodynamic stability calculations could help to predict the preferred binding mode.

It should be marked that in the IR spectrum of *Hhnc* (experimentally accessible) the first intense band in the 2000–500 cm$^{-1}$ region is attributed to $\nu$(C3O4) mode and the $\nu$(C3O4) frequency shift could indicate the ligand binding mode in the metal complexes. The calculated $\nu$(C3O4) frequency is at 1841 cm$^{-1}$ (Fig. 7) and it is used in the comparative vibrational analysis below. The intense $\nu$(C3O4) band shifts to lower frequency by ~30 and ~40 cm$^{-1}$ in the bidentate O1,O2-Cu(I)hnc1 and bidentate O2,O3-Cu(I)hnc3 complexes, respectively (the carbonyl C3O4 group is free). For the bidentate O3,O4-Cu(I)hnc2 and monodenate O4-Cu(I)hnc4 complexes (the carbonyl C3O4 group is coordinated) the band shifts to lower frequencies by ~240 and ~213 cm$^{-1}$,

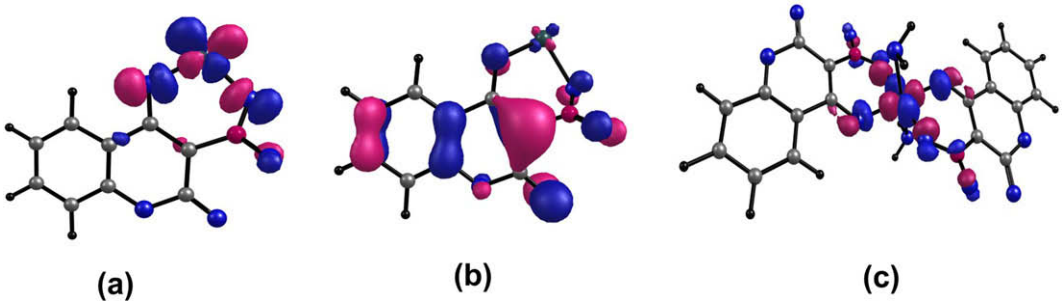


**Fig. 5.** HOMO of Cu(I)hnc1 complex (a), open shell orbitals of Cu(II)hnc1 (b) and $Cu(hnc)_2(H_2O)_2$ (c) at B3LYP level.

respectively. It the last two cases, the $\nu$(C3O4) band is the second one and its high intensity explicitly distinguishes it from the first $\nu$(C1O1) band. In summary, large downshift (above 200 $cm^{-1}$) and increasing intensity of the first band in the 2000–500 $cm^{-1}$ re-

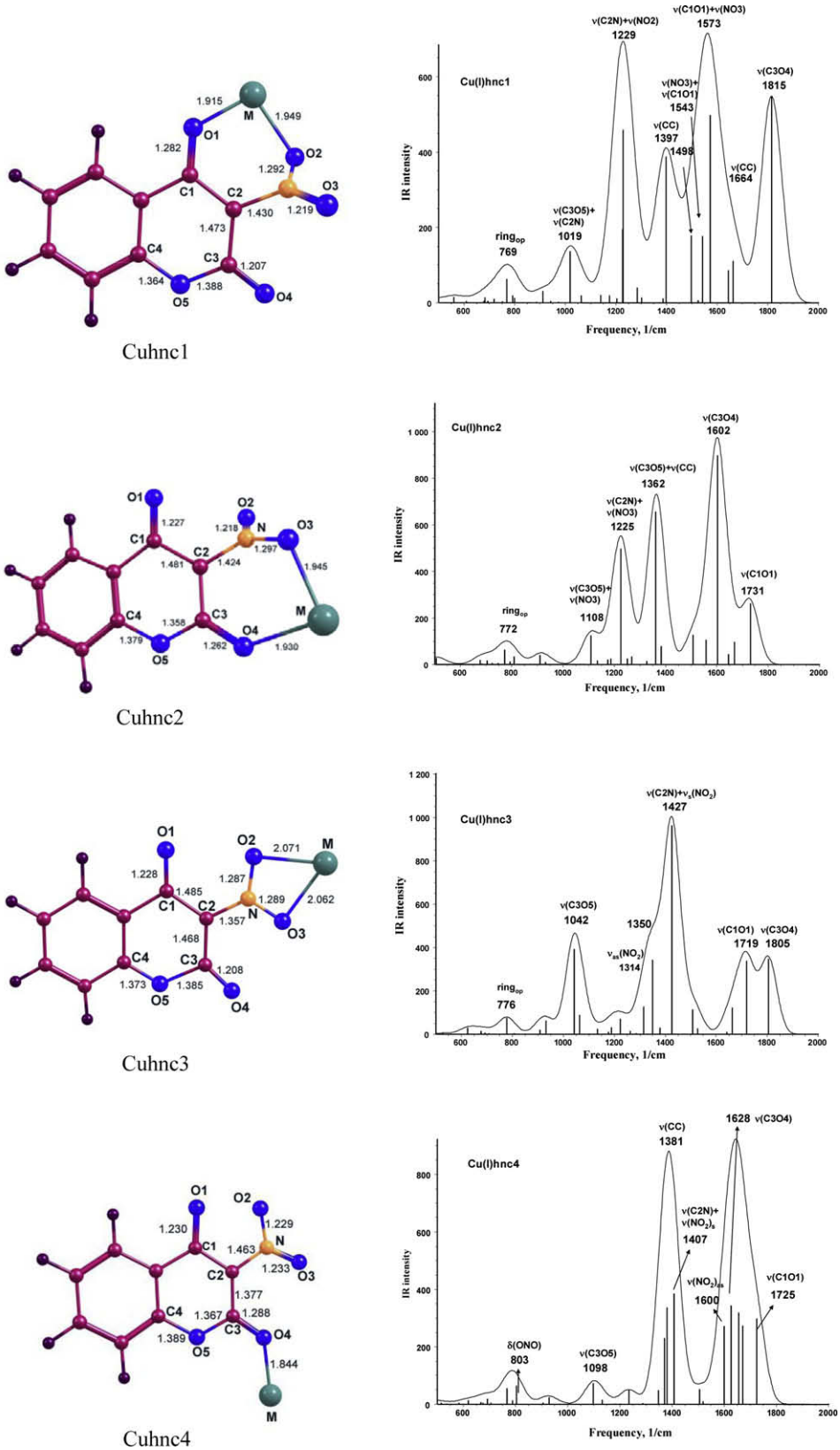


**Fig. 6.** Selected calculated bond lengths and IR wavenumbers (unscaled) of optimized Cu(I)hnc model complexes in different binding modes.

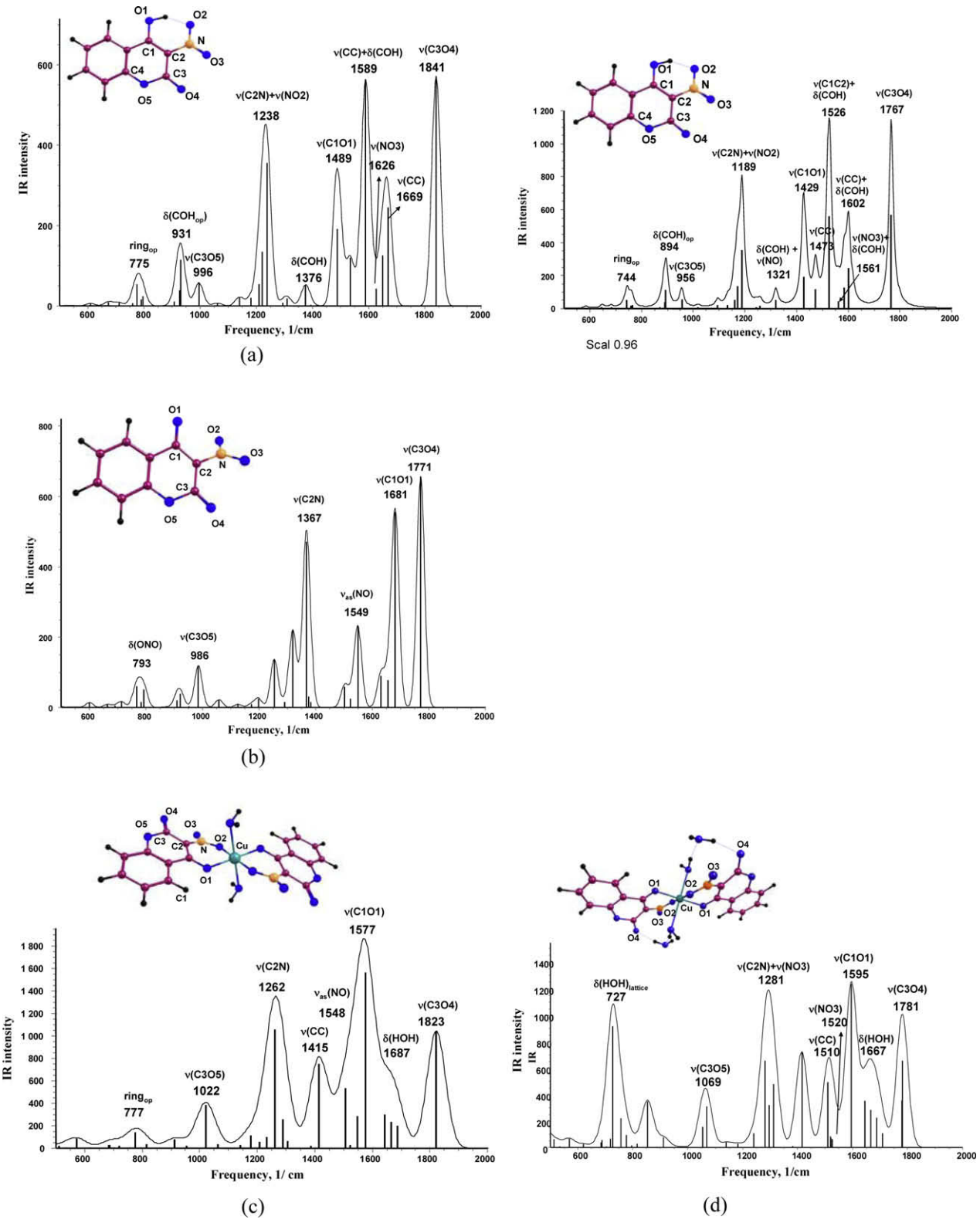


**Fig. 7.** Calculated IR spectra of *Hhnc* (a), *hnc*$^-$ (b), $Cu(hnc)_2(H_2O)_2$ (c) and $Cu(hnc)_2(H_2O)_2{\cdot}2H_2O$ (d).

gion of the metal complex as compared to the IR spectrum of *Hhnc* should be taken as an indication of coordinated carbonyl C═O group to the metal ion, whereas smaller band downshift ($\sim$35 cm$^{-1}$) and decreasing intensity denote uncoordinated carbonyl C═O group in the metal complexes.

### 3.3. Vibrational analysis of Hhnc, hnc$^-$ and its Cu(II) and Ag(I) complexes

The geometry and the vibrational spectra of *Hhnc*, *hnc*$^-$, $Cu(hnc)_2(H_2O)_2$, $Cu(hnc)_2(H_2O)_2{\cdot}2H_2O$, and Ag(hnc) are calculated

(Table 1) and discussed to explain: (1) the similarity of the IR spectra of Cu(II) and Ag(I) complexes (despite the different coordination) and (2) the downshift of $\nu$(C3O4) band (70 $cm^{-1}$) going from the *Hhnc* to its metal complexes (although this group is not coordinated in Cu(II) complex and it is monodenate (bridging) coordinated in Ag(I) complex). The clarification of the origin of the carbonyl (C=O) downshift and its magnitude is important since some authors used this shift as an evidence for complexation through the carbonyl oxygen atom [20,39]. By means of model calculations and comparative vibrational analysis presented below we intend to find a vibrational criterion for discernment of the free, H-bonded and coordinated carbonyl C=O group.

The calculated IR spectrum of the optimized *Hhnc* structure is presented in Fig. 7, compared with the experimental one (Table 1, Fig. 8a) [22]. To achieve better coincidence with the experimental vibrational frequencies (Fig. 8a), the calculated IR wavenumbers of *Hhnc* have been corrected by scaling factor of 0.96, Fig. 7a. The scaling factor is derived from the relation $\nu$(C3O4)exp/$\nu$(C3O4)calc. According to the calculations, the observed intense band (doublet) at 1760 $cm^{-1}$ (sc calc. 1767 $cm^{-1}$) is assigned to $\nu$(C3O4) stretching mode. The experimental IR band at 1608 $cm^{-1}$ (sc. calc. 1602 $cm^{-1}$) is due to the $\nu$(CC) mode. The calculated 1561 $cm^{-1}$ frequency, interpreted as $\nu$(NO3) vibration is not observed in the experimental IR spectrum due to its low intensity. Two modes, $\nu$(C1C2) and $\delta$(COH) contribute to the third intense band (doublet) at 1542 $cm^{-1}$ (sc. calc. 1526 $cm^{-1}$). The experimental bands at 1432 (sc. calc. 1429 $cm^{-1}$) and 1425 $cm^{-1}$ (sc. calc. 1428 $cm^{-1}$) are assigned to $\nu$(C1O1) and $\delta$(COH) modes, respectively. The intense band at 1192 $cm^{-1}$ (sc. calc. 1189 $cm^{-1}$) is assigned to $\nu$(C2N) + $\nu$(NO2) modes. The IR spectrum of $hnc^-$ is simulated via model calculations and it is presented in Fig. 7b. A survey of the geometrical and vibrational characteristics for *Hhnc* and $hnc^-$ (given in Table 1 and Fig. 7) reveals significant differences, originating from the breaking of the intramolecular hydrogen bond and hydroxyl deprotonation. The (H···O2) hydrogen bond is evaluated of 13 kcal/mol and its rupture produces an elongation of carbonyl C3=O4 bond (~0.004 Å) and downshift of $\nu$(C3O4) frequency by ~20 $cm^{-1}$. The H-bonding effect on the geometry and the $\nu$(C3O4) vibrational mode of *Hhnc* was estimated by comparison of the H-bonded *Hhnc* and non-H-bonded *Hhnc* conformer obtained from *Hhnc* by rotation around the C1–O1 bond of angle of 180° and subsequent unconstrained DFT optimization. Going from *Hhnc* to $hnc^-$ (including H-bond rupture and hydroxyl group deprotonation) the C1–O1, N–O2 and C2–C3 bonds shorten (the largest shortening of 0.07 Å is found for hydroxyl C1–O1 bond) and C1–C2, C2–N, N–O3, C3=O4, C3–O5 bonds elongate (the largest elongation of ~0.034 Å is found for C1–C2 bond). As a result, the carbonyl $\nu$(C3O4) band in $hnc^-$ downshifts by 70 $cm^{-1}$, whereas the hydroxyl $\nu$(C1O1) band is upshifted by 192 $cm^{-1}$. For qualitative estimation of the theoretical data obtained we discuss below the unscaled calculated spectra.

The modeling of $Cu(hnc)_2(H_2O)_2$ and $Cu(hnc)_2(H_2O)_2{\cdot}2H_2O$ complexes is performed on the basis of the coordination polyhedron obtained from X-ray diffraction analysis, Fig. 9 [22]. The last model complex includes two lattice water molecules (each one is H-bonded to the carbonyl oxygen and to the H atom of the coordinated water molecule) and thus it better approaches the experimental X-ray structure [22]. Selected bond lengths and stretching frequencies are given in Table 1 and Fig. 7c and d, respectively. According to the calculations the observed intense bands in the IR spectrum of the $Cu(hnc)_2(H_2O)_2{\cdot}2H_2O$ complex (Fig. 8b) were assigned as follow: at 1686 $cm^{-1}$ (calc. 1781 $cm^{-1}$) to $\nu$(C3O4); at 1552 $cm^{-1}$ (calc. 1595 $cm^{-1}$) to $\nu$(C1O1); at 1528 $cm^{-1}$ (calc. 1520 $cm^{-1}$) to $\nu$(NO3); at 1283 $cm^{-1}$ (calc. 1281 $cm^{-1}$) to $\nu$(NO2) + $\nu$(CN).

Firstly, the ligand frequency changes that occur upon bidentate bonding to Cu(II) through the hydroxyl and nitro oxygens (O1, O2) are studied by means of model calculations of $Cu(hnc)_2(H_2O)_2$. The calculations predicted the following wavenumbers for carbonyl $\nu$(C3O4): 1841 $cm^{-1}$ for *Hhnc*, 1771 $cm^{-1}$ for $hnc^-$ and 1823 $cm^{-1}$ for $Cu(hnc)_2(H_2O)_2$, Fig. 7. The $\nu$(C3O4) frequency variations follow the C3=O4 bond length variations in the compounds studied (Table 1). After H-bond breaking and ligand deprotonation, the carbonyl C3=O4 bond elongates and the $\nu$(C3O4) frequency downshifts by 70 $cm^{-1}$. Further, the coordination of $hnc^-$ through O1 and O2 atoms to Cu(II) produces shortening of C3=O4 bond and upshifted band by ~50 $cm^{-1}$. As a result, $\nu$(C3O4) band in $Cu(hnc)_2(H_2O)_2$ is shifted to lower frequencies (~20 $cm^{-1}$) as compared to that in *Hhnc*. If the intramolecular H-bond is missing in *Hhnc*, similar $\nu$(C3O4) frequencies are expected for *Hhnc* and $Cu(hnc)_2(H_2O)_2$.

A comparison of the vibrational spectra of the optimized $Cu(hnc)_2(H_2O)_2$ and $Cu(hnc)_2(H_2O)_2{\cdot}2H_2O$ shows that the H-bonding between the carbonyl C3O4 group and the lattice water leads

**Table 1**
Selected calculated and experimental bond lengths (in Å) and frequencies ($\nu$, in $cm^{-1}$) of *Hhnc*, $hnc^-$ and its Cu(II) and Ag(I) complexes at B3LYP/B1 level.

| System | C1–O1 | | C3–O4 | | N–O2 (C2–N) | | N–O3 | | C3–O5 | |
|---|---|---|---|---|---|---|---|---|---|---|
| | Bond | $\nu$ | Bond | $\nu$ | Bond | $\nu$[a] | Bond | $\nu$ | Bond | $\nu$[a] |
| *Hhnc* | 1.317 | 1489 [1429]$_{sc}$[c] | 1.203 | 1841 [1767]$_{sc}$ | 1.271 | 1238 [1189]$_{sc}$ | 1.218 | 1626 [1561]$_{sc}$ | 1.400 | 996 (956)$_{sc}$ |
| *Hhnc* (exp) | – | 1432s,d | – | 1760s,d | – | 1192s | | Overlap | | 918 |
| $hnc^-$ | 1.245 | 1681 (192)[d]↑ | 1.220 | 1771 (70)↓ | 1.239 | 1367 | 1.240 | $1549_{as}$ | 1.421 | 986 |
| $Cu(hnc)_2(H_2O)_2$ | 1.274 | 1592 | 1.205 | 1823 | 1.291 | 1262 | 1.222 | 1548 | 1.393 | 1022 |
| | 1.274 | 1577 (88–103)↑ | 1.205 | 1823 (18)↓ | 1.291 | 1246 | 1.222 | 1547 | 1.393 | 1021 |
| $Cu(hnc)_2(H_2O)_2{\cdot}2H_2O$ | 1.267 | 1607 | 1.217 | 1781 | 1.283 | 1282 | 1.229 | 1521 | 1.375 | 1070 |
| | 1.267 | 1595 [1541]$_{sc}$ | 1.217 | 1780 [1719]$_{sc}$ | 1.283 | 1262 | 1.229 | 1520 | 1.377 | 1069 |
| $Cu(hnc)_2(H_2O)_2{\cdot}2H_2O$ exp [22] | 1.258 | 1552vs (120)↑ | 1.216 | 1686vs (74)↓ | 1.232 | 1283vs | 1.218 | 1528sh | 1.369 | 1056m |
| | 1.257 | | 1.219 | | 1.246 | | 1.226 | | 1.369 | |
| Aghnc (PW91/PAW)[e] | 1.258 | 1572, 1560 (71)↑ | 1.240 | 1656, 1645 (196)↓ | 1.265 | 1289, 1288 | 1.265 | 1413 | 1.378 | 1042 |
| | | 1559, 1558 (69)↑ | | 1638, 1637 (204)↓ | | 1286, 1276 | | 1399 | | 1039 |
| | | | | | | | | 1398 | | |
| Aghnc exp [22] | 1.239 | 1584 (152)↑ | 1.223 | 1687 (73)↓ | 1.241 | 1285 | 1.242 | 1466 | 1.369 | 1042 |

vs – very strong; s – strong; d – doublet, sh – shoulder; as – asymmetric vibration; sc – scaled frequency.
[a] Coupling of $\nu$(NO2) and $\nu$(C2N) vibrations/coupling of $\nu$(C3O5) and $\nu$(C2N) vibrations.
[c] Scaling factor 0.96.
[d] The values in the brackets are the differences between the frequencies of the metal complexes and *Hhnc*.
[e] Periodic PW91/PAW optimization and frequency calculations are performed with VASP program.

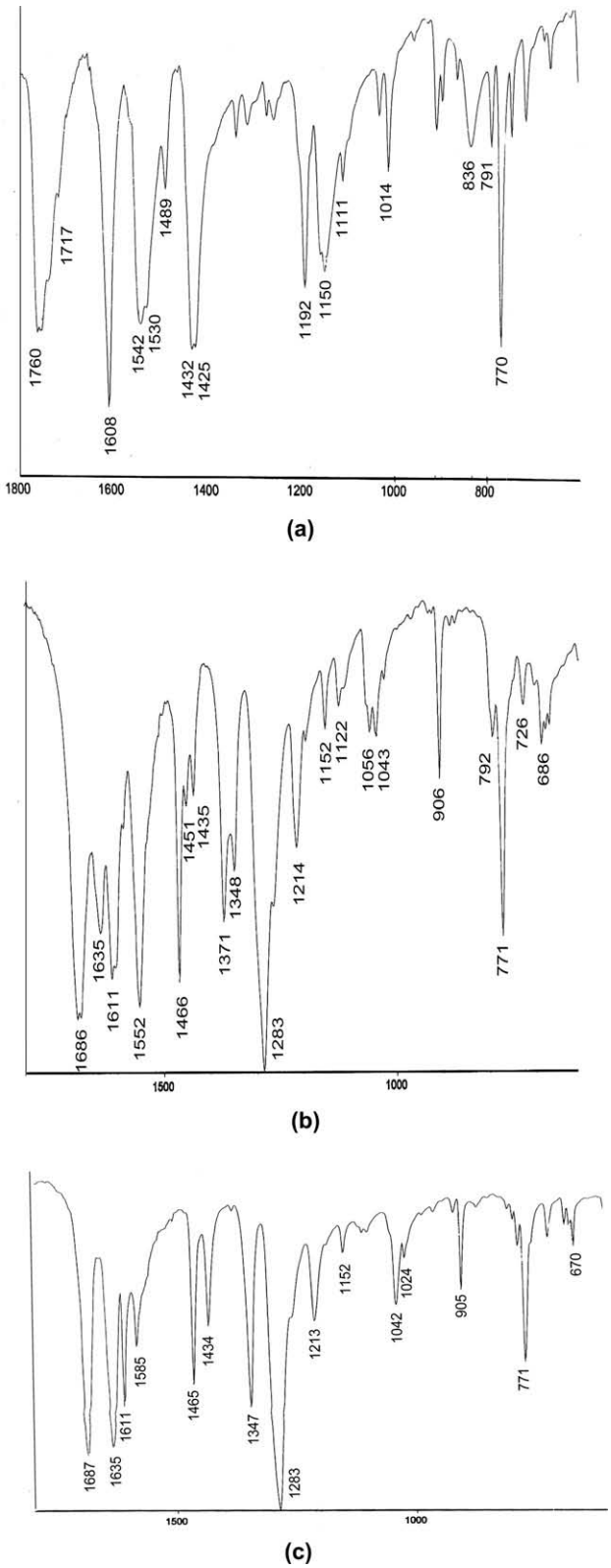


**Fig. 8.** Experimental IR spectra (in Transmittance, %) of *Hhnc* (a), $Cu(hnc)_2(H_2O)_2 \cdot 2H_2O$ (b) and Aghnc (c) [22].

to additional downshift of the $\nu$(C3O4) band by ~40 $cm^{-1}$ (bond length increases with 0.012 Å) and upshift of hydroxyl $\nu$(C1O1) band by ~15 $cm^{-1}$, Table 1 and Fig. 7c and d. According to the calculations of *Hhnc* and $Cu(hnc)_2(H_2O)_2 \cdot 2H_2O$ (or $Cu(hnc)_2(H_2O)_2$), the bands at 1432 $cm^{-1}$ in the ligand spectrum and that at 1552 $cm^{-1}$ in its Cu(II) complex are assigned to hydroxyl $\nu$(C1O1) mode (Table 1, Fig. 8a and b). As it is seen, the $\nu$(C1O1) band behaviour does not indicate explicitly that C1O1 group bounds to Cu(II) in the complex studied. The calculated $hnc^-$ IR spectrum, predicting $\nu$(C1O1) frequency at 1681 $cm^{-1}$, appears more reliable and informative for comparison with the IR spectrum of Cu(II) complex. Such a comparison shows that hydroxyl $\nu$(C1O1) band downshifts in the $Cu(hnc)_2(H_2O)_2$ complex by ~100 $cm^{-1}$ (1681 $cm^{-1}$ → 1595 $cm^{-1}$ (1575 $cm^{-1}$)) indicating C1O1 bonding to Cu(II) atom.

In summary, both bidentate bonding of $hnc^-$ through the hydroxyl and the nitro oxygens (O1, O2) and the H-bonding of lattice water to carbonyl C3O4 group in Cu(II) complex result in downshifted $\nu$(C3O4) band by ~60 $cm^{-1}$ as compared to that of *Hhnc*. This finding is consistent with the experimental difference, $\Delta \sim 45$–$75$ $cm^{-1}$ [22]. Therefore, such a downshift of $\nu$(C3O4) band could not be considered as an indication of coordination of the carbonyl C3O4 group to the metal ion. In case of coordinated carbonyl group, bidentate (Cuhnc2, Fig. 6) or monodentate (Cuhnc4, Fig. 6), our model calculations predicted larger downshift of $\nu$(C3O4) band by ~230 $cm^{-1}$ (~180 $cm^{-1}$ in Ag(I) complexes) as compared to that of *Hhnc*.

The Aghnc complex is polymeric, the Ag(I) being bonded to four coumarin molecules. One $hnc^-$ molecule is bidentately bonded to Ag(I) through the hydroxyl and nitro oxygens (O1, O2); two other $hnc^-$ molecules are bonded through the comarinic oxygen (O4) and the fourth $hnc^-$ molecule is bonded through the C atom, Fig. 9b [22]. The calculations of $Ag(hnc)_4$ model gave inadequate results. Thus, we performed periodic DFT calculations of Aghnc complex using the known unit cell parameters $a = 8.8770$ Å, $b = 6.7120$ Å, $c = 14.4640$ Å and $\beta = 101.899°$ and four formula units per unit cell, Table 1. In Aghnc complex the $hnc^-$ is a bridging ligand, bidentately bonded to one Ag(I) through the hydroxyl and the nitro oxygens (O1, O2) (as in Cu(II) complex) and monodentate bonded to another Ag(I) through the carbonyl O4. At the same time, the experimental IR spectra of Cu(II) and Ag(I) complexes showed very similar $\nu$(C3O4) frequencies at ~1686 $cm^{-1}$, Fig. 8b and c [22]. The crystallographic data showed similar C3=O4 bond lengths in Cu(II) and Ag(I) complexes (1.216 (1.219 Å) and 1.223 Å, respectively) in despite of the different bindings. Both complexes have bidentate (O1, O2) binding, therefore the lattice water H-bonded to carbonyl C3O4 group in Cu(II) complex and the Ag(I) bonded to C3O4 group in Ag(I) complex produce analogous changes in C3=O4 bond lengths and $\nu$(C3O4) frequencies. Our simulations of monodentate carbonyl oxygen binding to Cu(I)/Ag(I) (M(I)hnc4 model) showed that $\nu$(C3O4) band in *Hhnc* downshifts by ~210/185 $cm^{-1}$ and such a large $\nu$(C3O4) band shift could be accepted as an indication of monodentate carbonyl O4 binding. The observed binding through O4 does not produce the expected large band shift by ~180 $cm^{-1}$ since $hnc^-$ is bridging in Ag(I) complex: it is bonded to Ag1 through O1, O2 and to Ag2 through O4 atom.

In summary, the $\nu$(C3O4) band downshift by 30–90 $cm^{-1}$ in the IR spectra of the metal complexes as compared to this of the neutral *Hhnc* ligand should be taken as an indication of hydrogen bonded carbonyl (C3O4) group with lattice water molecules or bridged $hnc^-$ ligand in the complex and carbonyl oxygen binding to a metal ion. Significantly larger $\nu$(C3O4) band downshift by 180–240 $cm^{-1}$ should be attributed to monodentate ligand binding to the metal ion through the carbonyl group or bidentate ligand binding through the carbonyl and nitro groups.

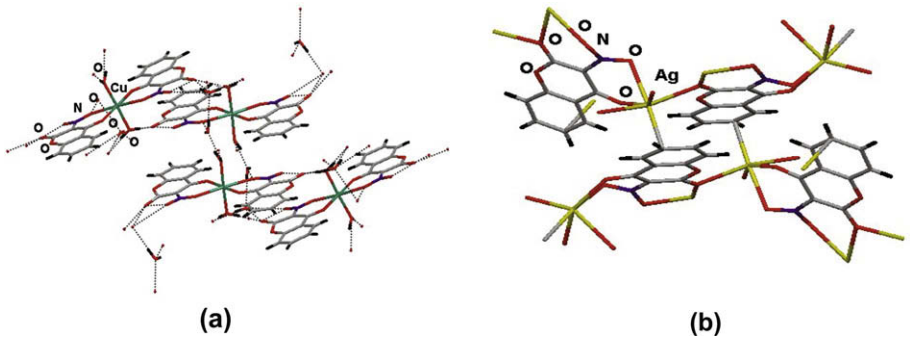


**Fig. 9.** Visualization of structures of $Cu(hnc)_2(H_2O)_2{\cdot}2H_2O$ (a) and Aghnc (b) complexes obtained from X-ray diffraction analysis [22].

## 4. Conclusion

The IR spectra of 4-hydroxy-3-nitro-*2H*-chromen-2-one (Hhnc) and its $Cu(hnc)_2(H_2O)_2{\cdot}2H_2O$ and $Ag(hnc)_4$ complexes were interpreted on the basis of B3LYP/B1 calculations in gas phase and PW91/PAW calculations in solid state (for Ag(I) complex). Geometrical, electronic and frequency calculations of model anionic ligand ($hnc^-$) and its $Cu(hnc)_2(H_2O)_2$, $Cu(hnc)_2(H_2O)_2{\cdot}2H_2O$ and Aghnc complexes explained the observed frequency downshift of the uncoordinated carbonyl group going from the free ligand to the metal complex as well as the similarity of the IR spectra of Cu(II) and Ag(I) complexes with different ligand coordination. The calculated MEP data and the relative stability of the models studied predicted the most preferred binding mode of $hnc^-$ to Cu(II), Cu(I) and Ag(I), namely a bidentate one via the hydroxyl and the nitro oxygens, in agreement with the experiment [22]. Based on the precisely selected Cu(I)hnc and Ag(I)hnc models, a relation between the vibrational behaviour of the ligand donor groups and the ligand binding modes in the complexes was deduced. It was suggested that the ligand coordination to a metal ion through the carbonyl group (monodentate or bidentate in combination with nitro group) produces large downshift (220–240 $cm^{-1}$) of the carbonyl stretching frequency. The comparative vibrational analysis showed that smaller downshift by 50–90 $cm^{-1}$ of the carbonyl frequency is due to intermolecular H-bonding of this group to the lattice water molecules or suggests a bridging $hnc^-$ ligand and binding of the carbonyl oxygen to the metal ion.

## Acknowledgements

The authors thank the National Science Fund of Bulgaria for the financial support (Grant Nos. DO-02-233 and DO-02-82). The calculations were performed on the computer cluster of the Institute of General and Inorganic Chemistry of the Bulgarian Academy of Sciences.

## Appendix A. Supplementary material

Supplementary data associated with this article can be found, in the online version, at doi:10.1016/j.chemphys.2009.10.004.

## References

[1] J.S. Seixas de Melo, R.S. Becker, A.L. Macanita, J. Phys. Chem. 98 (1994) 6054.
[2] M. Hoshiyama, K. Kubo, T. Igarashi, T. Sakurai, J. Photochem. Photobiol. 138 (2001) 227.
[3] H.E. Katerinopoulos, Curr. Pharm. Design 10 (2004) 3835.
[4] J.W. Suttie, Clin. Cardiol. 13 (VI) (1990) 16.
[5] A.H. Bedair, N.A. El-Hady, M.S. Abd El-Latif, A.H. Fakery, A.M. El-Agrody, I1 Farmaco 55 (2000) 708.
[6] P. Laurin, M. Klich, C. Dupis-Hamelin, P. Mauvais, P. Lassaigne, A. Bonnefoy, B. Musicki, Bioorg. Med. Chem. Lett. 9 (1999) 2079.
[7] G.J. Finn, B.S. Creaven, D.A. Egan, Cancer Lett. 214 (2004) 43.
[8] G.J. Finn, B.S. Creaven, D.A. Egan, Biochem. Pharmacol. 67 (2004) 1779.
[9] G.J. Finn, B.S. Creaven, D.A. Egan, Eur. J. Pharm. Sci. 26 (2005) 16.
[10] M.E. Marshall, M. Ryles, K. Butler, L. Weiss, J. Cancer Res. Clin. Oncol. 120 (1994) 535.
[11] T. Patonay, G. Litkei, R. Bognar, J. Eredi, C. Miszti, Pharmazie 39 (1984) 86.
[12] P. Tiew, J.R. Ioset, U. Kokpal, W. Chavasiri, K. Hostettmam, Phytother. Res. 17 (2003) 190.
[13] B. Thati, A. Noble, R. Rowan, B.S. Creaven, M. Walsh, M. McCann, D.A. Egan, K. Kavanagh, Toxicol. In Vitro 21 (2007) 801.
[14] R.J.S. Hoult, M. Paya, Gen. Pharmacol. 27 (1996) 713.
[15] S.P. Pillai, S.R. Menon, L.A. Mitscher, C.A. Pillai, D.A. Shankel, J. Nat. Prod. 62 (1999) 1358.
[16] B. Thati, A. Noble, B.S. Creaven, M. Walsh, M. McCann, K. Kavanagh, M. Devereux, D.A. Egan, Cancer Lett. 248 (2007) 321.
[17] B.S. Creaven, D.A. Egan, D. Karcz, K. Kavanagh, M. McCann, M. Mahon, A. Noble, B. Thati, M. Walsh, J. Inorg. Biochem. 101 (8) (2007) 1108.
[18] S. Creaven, D.A. Egan, K. Kavanagh, M. McCann, A. Noble, B. Thati, M. Walsh, Inorg. Chim. Acta 359 (2006) 3976.
[19] H. Sakurai, Y. Kojima, Y. Yoshikawa, K. Kawabe, H. Yasui, Coord. Chem. Rev. 226 (2002) 187.
[20] (a) I. Kostova, I. Manolov, I. Momekov, Eur. J. Med. Chem. 39 (2004) 765;
(b) I. Kostova, G. Momekov, M. Zaharieva, M. Karaivanova, Eur. J. Med. Chem. 40 (2005) 542.
[21] K.B. Guadasi, R.V. Shenoy, R.S. Vadavi, M.S. Patil, S.A. Patil, Chem. Pharm. Bull. 53 (9) (2005) 1077.
[22] B.S. Creaven, D.A. Egan, K. Kavanagh, M. McCann, M. Mahon, A. Noble, B. Thati, M. Walsh, Polyhedron 24 (2005) 949.
[23] I. Georgieva, I. Kostova, N. Trendafilova, V.K. Rastogi, G. Bauer, W. Kiefer, J. Raman Spectrosc. 37 (7) (2006) 742.
[24] Tz. Mihaylov, N. Trendafilova, I. Kostova, I. Georgieva, G. Bauer, Chem. Phys. 327 (2006) 209.
[25] Tz. Mihaylov, I. Georgieva, G. Bauer, I. Kostova, I. Manolov, N. Trendafilova, Int. J. Quantum Chem. 106 (6) (2006) 1304.
[26] I. Georgieva, Tz. Mihaylov, G. Bauer, N. Trendafilova, Chem. Phys. 300 (2004) 119.
[27] I. Georgieva, N. Trendafilova, W. Kiefer, V.K. Rastogi, I. Kostova, Vib. Spectrosc. 44 (1) (2007) 78.
[28] M.J. Frisch, G.W. Trucks, H.B. Schlegel, G.E. Scuseria, M.A. Robb, J.R. Cheeseman, J.A. Montgomery, Jr., T. Vreven, K.N. Kudin, J.C. Burant, J.M. Millam, S.S. Iyengar, J. Tomasi, V. Barone, B. Mennucci, M. Cossi, G. Scalmani, N. Rega, G.A. Petersson, H. Nakatsuji, M. Hada, M. Ehara, K. Toyota, R. Fukuda, J. Hasegawa, M. Ishida, T. Nakajima, Y. Honda, O. Kitao, H. Nakai, M. Klene, X. Li, J.E. Knox, H.P. Hratchian, J.B. Cross, V. Bakken, C. Adamo, J. Jaramillo, R. Gomperts, R.E. Stratmann, O. Yazyev, A.J. Austin, R. Cammi, C. Pomelli, J.W. Ochterski, P.Y. Ayala, K. Morokuma, G.A. Voth, P. Salvador, J.J. Dannenberg, V.G. Zakrzewski, S. Dapprich, A.D. Daniels, M.C. Strain, O. Farkas, D.K. Malick, A.D. Rabuck, K. Raghavachari, J.B. Foresman, J.V. Ortiz, Q. Cui, A.G. Baboul, S. Clifford, J. Cioslowski, B.B. Stefanov, G. Liu, A. Liashenko, P. Piskorz, I. Komaromi, R.L. Martin, D.J. Fox, T. Keith, M.A. Al-Laham, C.Y. Peng, A. Nanayakkara, M. Challacombe, P.M.W. Gill, B. Johnson, W. Chen, M.W. Wong, C. Gonzalez, J.A. Pople, Gaussian 03, Revision B.05, Gaussian, Inc., Wallingford CT, 2004.
[29] C. Lee, W. Yang, R.G. Parr, Phys. Rev. B 37 (1988) 785.
[30] A.D. Becke, J. Chem. Phys. 98 (1993) 5648.
[31] (a) M. Dolg, H. Stoll, A. Savin, H. Preuss, Theor. Chim. Acta 75 (1989) 173;
(b) M. Dolg, P. Fulde, W. Kuechle, C.-S. Neumann, H. Stoll, J. Chem. Phys. 94 (1991) 3011;
(c) M. Dolg, H. Stoll, H. Preuss, Theor. Chim. Acta 85 (1993) 441.
[32] P. Fuentealba, H. Stoll, L.v. Szentpaly, P. Schwerdtfeger, H. Preuss, J. Phys. B 16 (1983) L323.
[33] Available from <http://www.chemcraftprog.com>.
[34] (a) G. Kresse, J. Hafner, Phys. Rev. B 47 (1993) RC558;
(b) G. Kresse, Thesis, Technische Universität Wien, 1993.;

(c) G. Kresse, J. Furthmüller, Comput. Mat. Sci. 6 (1996) 15;
(d) G. Kresse, J. Furthmüller, Phys. Rev. B 54 (1996) 11169.
[35] J.M. Campanario, E. Bronchalo, M.A. Hidaigo, J. Chem. Edu. 71 (9) (1994) 761.
[36] J. Tomasi, in: P. Politzer, D.G. Truhlar (Eds.), Chemical Applications of Atomic and Molecular Electrostatic Potentials, Plenum Press, New York, 1981, p. 257.
[37] (a) M. Noguera, J. Bertran, M. Sodupe, J. Phys. Chem. B 112 (2008) 4817;
(b) M. Noguera, J. Bertran, M. Sodupe, J. Phys. Chem. A 108 (2004) 333.
[38] (a) C. Trujillo, Al M. Lamsabhi, O. Mó, M. Yáñez, Phys. Chem. Chem. Phys. 10 (2008) 3229;
(b) Al M. Lamsabhi, M. Alcamí, O. Mó, M. Yáñez, J. Tortajada, J.-Y. Salpin, ChemPhysChem 8 (2007) 181.
[39] (a) I. Kostova, I. Manolov, I. Nicolova, S. Konstantinov, M. Karaivanova, Eur. J. Med. Chem. 36 (2001) 339;
(b) I. Kostova, I. Manolov, M. Karaivanova, Arch. Pharm. Pharm. Med. Chem. 334 (2001) 157.